International Journal for Housing Science and Its Applications
Publish August 5, 2025. Volume 46, Issue 3 Pages 4227-4243

https://doi.org/10.70517/ijhsa463361

Research on coupling mechanism of groundwater flow and soil deformation in geotechnical engineering based on improved finite element method

Xilin Yao[1,*]
[1] Civil Engineering School, Wuhan University, Wuhan, Hubei, 430072, China
Corresponding authors: (e-mail: xilin041@gmail.com).

Abstract In order to better utilize the groundwater seepage field under artificial conditions as a technical tool, it is necessary to study the infiltration properties of soil, the infiltration law of groundwater in the soil layer and its relationship with engineering. Therefore, this paper takes the HM area as the study area according to its hydrogeological characteristics, and divides the aquifers into submersible aquifers as well as the Ⅰ, Ⅱ, and Ⅲ pressurized aquifers in order from top to bottom. The hydrogeological conceptual model was established, and the soil deformation direction was analyzed according to the Terzaghi effective stress principle to form a coupled groundwater flow-soil deformation model. On the basis of the finite element discretization method, the finite element governing equations of the Bio-consolidation theory are considered to be established by the Galyokin weighted residual method to solve the previously constructed coupling model. According to the method of model identification, the hydrogeological parameters of the study area are identified and calibrated, and the water storage rate of the Ⅰ pressurized aquifer is slightly higher than that of the Ⅱ pressurized aquifer, and the average value of the zonal water storage rate is 0.00007385, which is 0.00002048 higher than that of the Ⅱ pressurized aquifer. The coupled soil-moisture deformation analysis is carried out, and the average water content in the upper layer of the lower sand basically agrees with the change of vertical deformation, and the 0- 5h average water content decreased from 23% to 17%, after 5h in a stable state, it can be seen that pumping - recharge this process, the soil structure in the two stages of compression deformation, will reach a relatively stable state.

Index Terms hydrogeological conceptual model, Terzaghi effective stress, coupled water flow-soil deformation model, finite element discretization, occlusion theory

I. Introduction

In the process of geotechnical engineering investigation, design and construction, hydrogeology is always an extremely important but also an easy to be ignored problem [1]. In some areas with complicated hydrogeological conditions, due to the lack of in-depth study of hydrogeological problems in engineering investigation and the neglect of hydrogeological problems in design, a variety of geotechnical engineering hazards triggered by groundwater often occur, which puts the investigation and design in an embarrassing situation [2]-[5]. Groundwater is an important factor in inducing soil deformation, especially in areas where groundwater is particularly abundant [6]. The flow of groundwater changes the stress state as well as the mechanical properties of the rock and structural surfaces within the soil body, leading to large changes in the stability of the soil body, resulting in extensive deformation of the soil body in the region [7]-[9].

Therefore, groundwater flow has a greater impact on the excavation and support of geotechnical engineering, if the groundwater problem can not be dealt with in time, it may lead to different degrees of settlement and deformation of the soil body and the surrounding building structure, and in serious cases, it may even cause huge economic losses and engineering safety accidents [10]-[13]. In order to improve the quality of geotechnical engineering construction, it is not only required to identify the hydrogeological problems related to geotechnical engineering, evaluate the role of groundwater on the geotechnical body and buildings and its influence, but also to propose the recommendations of preventive and treatment measures in engineering investigation [14]-[16]. Through the establishment of simulation models, the deformation mechanism of soil engineering under the coupling of seepage field and stress field is explored to provide necessary hydrogeological information for design and construction, so as to eliminate or reduce the hazards of groundwater on geotechnical engineering [17]-[19].

In this paper, taking the HM area as an example, the aquifers in the study area are divided into submersible aquifers as well as the Ⅰ, Ⅱ and Ⅲ pressurized aquifers in order from top to bottom, with reference to the information of the geological conditions in the area, the proposed three-dimensional directional stress field and seepage field full-coupling model is established. According to Terzaghi effective stress principle, the deformation direction of soil body is calculated according to three-dimensional consolidation theory. The three-dimensional groundwater flow one-dimensional soil deformation coupling model is constructed, the seepage finite element discretization equations are established according to the variational principle, and the finite element governing equations of the Bio-consolidation theory are set up using the Galyokin weighted residual method to solve the groundwater flow-soil deformation coupling model. Through simulation experiments, the rationality of the identified hydrogeological parameters is verified, and based on the coupled soil-moisture deformation analysis data, the coupling analysis is carried out to study the mechanism.

II. Coupling mechanism of groundwater flow and soil deformation in geotechnical engineering

II. A. Area profile and hydrogeologic conceptual modeling

II. A. 1) Regional overview

The HM District of NT is located in the southeastern part of Jiangsu Province, bordering the Yellow Sea to the east and the Yangtze River to the south, and is situated at latitude 31°46′-32°09′N and longitude 121°04′-121°32′E, with a land area of 1,148.77km².The average annual temperature is 15.6°C, with an extreme minimum temperature of -9.3°C, and the maximum temperature is 38.0°C. The average annual precipitation in the HM area is 1040.4 mm, and the annual precipitation is greater than 850.0 mm in 78% of the years. According to the hydrogeological characteristics, the aquifers in the study area are classified as submersible aquifers and Ⅰ, Ⅱ, Ⅲ pressurized aquifers from top to bottom, and the corresponding geological ages are Q_4 (Holocene), Q_3 (Upper Pleistocene), Q_2 (Middle Pleistocene) and Q_1 (Lower Pleistocene) in order.

II. A. 2) Conceptual hydrogeological modeling

The planar scale of the HM zone is 46755 m × 38412 m, and the depth in the vertical direction is 230-350 m. The data on the geological conditions in this zone for many years show that the Tertiary porous sand layer is well cemented, and the buried depth of its aquifer is large, with a low utilization rate of the groundwater, which has a low degree of influence on the deformation of the soil body. Therefore, the proposed three-dimensional directional stress field and seepage field fully coupled model takes the ground surface as the upper boundary and the bottom plate of the Ⅲ pressurized aquifer as the lower boundary.

The large-scale exploitation of the Ⅲ pressurized aquifer in the study area in the previous period has led to a large decrease in the groundwater level in the city center, resulting in a strong hydraulic connection between the aquifers. Meanwhile water level observation data show that groundwater pressure mining was practiced in 2013 in the HM area. The groundwater level rebounded rapidly at the early stage of pressure mining, and with the passage of time, the rebound rate of the Ⅲ pressurized aquifer decreased, showing obvious non-stability. Therefore, the groundwater flow pattern is generalized to three-dimensional unsteady flow.

II. A. 3) Overview of soil deformation directions

According to Terzaghi's effective stress principle, if the total stress of the soil body is assumed to be constant, the decrease of pore water pressure in the soil body is equal to the increase of effective stress [20]. In this paper, the simulation calculation is carried out on the assumption that the soil body only produces deformation in the vertical direction, while the deformation in the horizontal direction is zero, and it is considered that the process of compacting and releasing water in clayey soil is also in line with the theory of one-dimensional consolidation of the Taishaghi base, i.e., the deformation of the soil body in the study area deforms one-dimensionally in the vertical direction.

II. B. Coupled modeling of groundwater flow and soil deformation

II. B. 1) Three-dimensional groundwater flow modeling

Based on the hydrogeological conceptual model established in 2.1.2, the groundwater flow in the study area is generalized to three-dimensional unsteady flow, and the corresponding three-dimensional unsteady flow mathematical model of groundwater movement is established [21].

$$\begin{cases} \mu \dfrac{\partial h}{\partial t} = K_{xx}\left(\dfrac{\partial h}{\partial x}\right)^2 + K_{yy}\left(\dfrac{\partial h}{\partial y}\right)^2 + K_z\left(\dfrac{\partial h}{\partial z}\right)^2 - \dfrac{\partial h}{\partial t}(K_z + p) + p & x, y, z \in \Gamma_0, t \geq 0 \\ \dfrac{\partial}{\partial x}\left(K_{xx}\dfrac{\partial h}{\partial x}\right) + \dfrac{\partial}{\partial y}\left(K_{yy}\dfrac{\partial h}{\partial y}\right) + \dfrac{\partial}{\partial z}\left(K_{zz}\dfrac{\partial h}{\partial z}\right) - W = S_s\dfrac{\partial h}{\partial t} & x, y, z \in \Omega, t \geq 0 \\ h(x, y, z, t)\,|_{t=0} = h_0 & x, y, z \in \Omega, t \geq 0 \\ \dfrac{K_r}{M_r}(H_r - H) = q(x, y, t) & x, y, z \in \Gamma_1, t \geq 0 \\ K_{\vec{n}}\dfrac{\partial h}{\partial \vec{n}}\,|_{\Gamma_2} = q(x, y, t) & x, y, z \in \Gamma_2, t \geq 0 \\ \dfrac{(h_r - h)}{\sigma} - K_n\dfrac{\partial h}{\partial z}\,|_{\Gamma_3} = 0 & x, y, z \in \Gamma_3, t \geq 0 \end{cases} \tag{1}$$

where: μ is the degree of gravity feed, h is the water level elevation of the aquifer, m, K_{xx} and K_{yy} are the horizontal permeability coefficients, m/d, K_{yy} is the vertical permeability coefficient, m/d, p is the evaporation and precipitation etc. of the submerged surface, m/d, Γ_0 is the upper boundary of the seepage region, i.e., the free surface of groundwater. S_s is the storage rate of the pressurized aquifer, 1/m, W is the source-sink term of the aquifer, 1/d. Ω is the seepage area, h_0 is the initial water level of the aquifer, m, K_r is the permeability coefficient of the streambed medium, m/d, M_r is the thickness of the stream bed medium, Γ_1 is the river boundary of the seepage region, and $\vec{n}$ is the normal direction on the boundary surface. $K_{\vec{n}}$ is the infiltration coefficient, m/d, in the normal direction on the boundary surface, Γ_2 is the class II boundary of the aquifer system, $q(x, y, t)$ is the flow rate passing through the unit area of the model boundary, with inflow of water being positive, and outflow of water being negative, and the value is 0 m/d at the watertight boundary, Γ_3 is the three types of boundaries of the seepage region, i.e., the generic head boundary.

II. B. 2) One-dimensional soil deformation models

(1) One-dimensional soil deformation theory

This part is realized with the help of SUB module in Modflow, which calculates the deformation amount of the interlayer in the simulation process of the module is based on the development of Terzaghi's one-dimensional consolidation theory, whose calculation process ignores the horizontal stress and only considers the vertical deformation of the soil body. Among them, the coupling of the deformation of the soil body with the head change applies Terzaghi's effective stress principle:

$$\Delta\sigma_{zz}^{'} = -\rho_w g \Delta h \tag{2}$$

where: $\sigma_{zz}^{'}$ is the vertical effective stress of soil, ρ_w is the density of pore water, Δh is the change of head of soil, and g is the gravitational acceleration of soil.

If the total stress on the aquifer does not change, then in the process of groundwater extraction, the pore water pressure of the aquifer decreases due to the decreasing water level, causing the effective stress on the water-bearing medium to increase, which leads to vertical compressive deformation of the soil skeleton of the aquifer. The soil compression coefficient α is introduced here to measure its compressibility, which means: when the effective stress of the soil skeleton particles change by one unit of change in the overall volume (thickness) of the porous media caused by the relative change:

$$\overline{a} = \frac{-\dfrac{dV}{V}}{d\sigma} = \frac{-\dfrac{db}{b}}{d\sigma_{zz}^{'}} \tag{3}$$

where: α is the compression coefficient of the soil body in the vertical direction, $d\sigma_{zz}^{'}$ is the change in the effective stress in the vertical direction, b is the initial vertical thickness of the soil body, and db is the change in the vertical thickness of the soil body.

It has already been explained that the water and soil skeleton particles are assumed to be incompressible during the calculation process, in which case the compressive deformation of the soil body can be approximated to be equal to the volume of water discharged when the head of the medium per unit of the aquifer drops by one unit. Here, the water storage rate of the soil skeleton is introduced and can be obtained by combining equations (1), (2), and (3):

$$\rho_w g\bar{a}b = S_{sk}b = S_s = \frac{db}{dh} \tag{4}$$

In general, Eq. (4) can be linearized as:

$$\Delta b = S_{sk}b\Delta h \tag{5}$$

where: $S_{sk} = \rho_w g\bar{\alpha}$ is the soil skeleton water storage rate, $S_s = S_{sk}b$ is the soil skeleton water storage coefficient, and Δb is the compressive deformation of the soil.

For the cumulative settlement at a point on the ground, it is first assumed in the calculation that all the interlayers below the point are spread horizontally, then the cumulative settlement due to water release from the interlayers at the point is equal to the sum of the compression of all the interlayers vertically upwards below the surface of the point, i.e.:

$$B = \sum_{i=1}^{n}\Delta b_i = b\sum_{i=1}^{n}S_{ki}\Delta h_i \tag{6}$$

The relationship between the pre-consolidation stress of the soil and the minimum water level of the aquifer is:

$$\sigma_0 = \sigma - \rho g h_0 \tag{7}$$

where: σ_0 is the pre-consolidation stress of the soil, and h_0 is the historical minimum water level of the aquifer.

Eq. (7) shows that when the water level of the aquifer is lower than its pre-existing minimum water level, the water-releasing compressive deformation of the soil body is plastic, while when the water level is higher than the pre-existing minimum water level, the water-releasing compressive deformation of the soil body belongs to elastic deformation. Therefore, the water storage rate of inelastic skeleton and the water storage rate of elastic skeleton are used to express the different stages of water release and compression deformation of clayey soil during the simulation process, and the equations are as follows:

$$S_{sk} = \begin{cases} S_{ske} = \dfrac{0.434C_r\rho_w}{\sigma_0(1+e_0)} & h^{'} > h_{\min} \\ S_{skv} = \dfrac{0.434C_c\rho_w}{\sigma_0(1+e_0)} & h^{'} < h_{\min} \end{cases} \tag{8}$$

where S_{ske} is the elastic soil skeleton water storage rate, S_{skv} is the inelastic skeleton water storage rate, $h_{\min}^{'}$ is the pre-consolidation water table, C_c is the soil compression coefficient, C_r is the soil resilience coefficient, and e_0 is the initial porosity ratio.

(2) Hysteresis treatment of soil deformation

The time required for the compression of the weakly permeable layer (interlayer) to reach 93% of its final settlement is τ_0 under the condition of determining the change in the head of the aquifer:

$$\tau_0 = \frac{(\frac{b_0}{2})^2 S_s^{'}}{K_v^{'}} \tag{9}$$

where: $S_s^{'}$ is the water storage rate of the interlayer in the aquifer, $K_v^{'}$ is the vertical permeability coefficient of the interlayer in the aquifer, and b_0 is the initial thickness of the interlayer.

II. B. 3) Three-dimensional groundwater flow and one-dimensional soil deformation coupled modeling

The groundwater flow in the study area is generalized to a three-dimensional unsteady flow with the following mathematical equations:

$$\frac{\partial}{\partial x}\left(K_{xx}\frac{\partial h}{\partial x}\right)+\frac{\partial}{\partial y}\left(K_{yy}\frac{\partial h}{\partial y}\right)+\frac{\partial}{\partial z}\left(K_{zz}\frac{\partial h}{\partial z}\right)-W=S_s\frac{\partial h}{\partial t} \tag{10}$$

Volume and the amount of change in storage volume of the aquifer. Assuming that the volume percentage of the interlayer to the whole aquifer system is γ, the right-hand term of Eq. (10) represents the amount of water per unit volume of water-bearing medium entering or leaving the aquifer per unit of time, i.e., the amount of change in the storage of the aquifer $\overline{q}=S_s\frac{\partial h}{\partial t}$. In this paper, the amount of change in storage of each grid can be divided into the right term of the storage change of the sandwich layer should be multiplied by the coefficient $(1-\gamma)$, which will be reduced to $(1-\gamma)S_s\frac{\partial h}{\partial t}$. In contrast, the amount of storage change in the entrapment, i.e., the amount of water that enters the aquifer from the entrapment or enters the entrapment from the aquifer, is usually represented by another expression. In calculating the amount of deformation of the entire aquifer system, the amount of storage change in the interlayer can be added to the right-hand term of Eq. (10).

Assuming that there are N "non-hysteresis interlayers" in an aquifer, then the soil skeleton water storage coefficient of the "non-hysteresis interlayer" composed of N "non-hysteresis interlayers" can be calculated by Eq. (8), and the change in the reserves of the "non-hysteresis interlayer" can be calculated by Eq. (12):

$$S_s^{'}=\sum_{i=1}^{N}S_{s_i}^{'}=\sum_{i=1}^{N}S_{sk_i}^{'}b_i \tag{11}$$

$$\overline{q}=\gamma S_{sk}^{'}\frac{\partial h}{\partial t} \tag{12}$$

$\overline{q}$ is the amount of change in the entrained reservoir, and by adding it to the source-sink term W in Eq. (10), the coupling of the three-dimensional groundwater flow model with the one-dimensional silhouette deformation model is realized.

In a sandwich system, assuming that the thickness of each "hysteresis interlayer" with the same vertical permeability coefficient is b_i, the thickness of each interlayer can be expressed by the equivalent interlayer thickness b_{equiv} (Equation 13), and the number of regenerated interlayers can be expressed by the equivalent number of interlayers n_{equiv} (Equation 14).

$$b_{equiv}=\sqrt{\frac{1}{N}\sum_{i}^{N}b_i^2} \tag{13}$$

$$n_{equiv}=\frac{\sum_{i}^{N}b_i}{b_{equiv}} \tag{14}$$

Based on Darcy's law, the storage change of the “lagging interlayer” can be calculated, and then the groundwater flow model can be coupled with the soil deformation model by adding the storage change of each interlayer, $\overline{q}$, into the source-sink term of Eq. (10):

$$\frac{\partial}{\partial x}\left(K_{xx}\frac{\partial h}{\partial x}\right)+\frac{\partial}{\partial y}\left(K_{yy}\frac{\partial h}{\partial y}\right)+\frac{\partial}{\partial z}\left(K_{zz}\frac{\partial h}{\partial z}\right)-(W+\overline{q})=(1-\gamma)S_s\frac{\partial h}{\partial t} \tag{15}$$

III. Based on groundwater flow and soil deformation coupling model finite element solution

III. A. Finite element discretization methods

III. A. 1) Discrete finite element equations for seepage flow

According to the variational principle, the percolation fixed solution problem in this paper is equivalent to the following generalized function taking minimal values:

$$I(h)=\iiint\limits_{\Omega}\left\{\frac{1}{2}\left[k_x\left(\frac{\partial h}{\partial x}\right)^2+k_y\left(\frac{\partial h}{\partial y}\right)^2+k_z\left(\frac{\partial h}{\partial x}\right)^2+S_s h\frac{\partial h}{\partial t}\right]\right\}dxdydz+\iint\limits_{\Gamma_s}qhd\Gamma \tag{16}$$

The region Ω is dissected hexahedrally, whereupon the integral over Ω can be reduced to a sum of integrals over each hexahedral cell, and the generalization Eq. (16) decomposes accordingly into a sum of the relevant cellular generalizations, viz:

$$\begin{aligned}I^e(h)&=\iiint\limits_{e}\left\{\frac{1}{2}\left[k_x(\frac{\partial h}{\partial x})^2+k_y(\frac{\partial h}{\partial y})^2+k_z(\frac{\partial h}{\partial x})^2+S_s h\frac{\partial h}{\partial t}\right]\right\}dxdydz+\iint_{\Gamma_2}qhd\Gamma\\&=I_1^e+I_2^e+I_3^e\end{aligned} \tag{17}$$

Taking the spatial 8-node isotropic hexahedral linear cell as an example, the corresponding form function is:

$$N_i(\xi,\eta,\xi)=\frac{1}{8}(1+\xi,\xi)(1+\eta,\eta)(1+\zeta,\xi)\quad(i=1,2,\cdots,8) \tag{18}$$

$$[N]=[N_1,N_2,\cdots,N_8] \tag{19}$$

where: $(\xi_i,\eta_i,\varsigma_i)$ is the coordinate of the corresponding node i on (ξ,η,ς). At this point the coordinate transformation formula on the cell is:

$$\begin{aligned}x&=\sum_{i=1}^{8}N_i(\xi,\eta,\varsigma)x_i\\y&=\sum_{i=1}^{8}N_i(\xi,\eta,\varsigma)y_i\\z&=\sum_{i=1}^{8}N_i(\xi,\eta,\varsigma)z_i\end{aligned} \tag{20}$$

The interpolation function of h on the cell is:

$$h=[N]\{h\}^e=\sum_{i=1}^{8}N_i(\xi,\eta,\varsigma)h_i \tag{21}$$

The partial derivative of the head h with respect to the overall coordinates is:

$$\begin{pmatrix}\frac{\partial h}{\partial x}\\\frac{\partial h}{\partial y}\\\frac{\partial h}{\partial z}\end{pmatrix}=\begin{bmatrix}\frac{\partial N_1}{\partial x}&\frac{\partial N_2}{\partial x}&\cdots&\frac{\partial N_8}{\partial x}\\\frac{\partial N_1}{\partial y}&\frac{\partial N_2}{\partial x}&\cdots&\frac{\partial N_8}{\partial y}\\\frac{\partial N_1}{\partial z}&\frac{\partial N_2}{\partial z}&\cdots&\frac{\partial N_8}{\partial z}\end{bmatrix}\begin{bmatrix}h_1\\h_2\\\vdots\\h_8\end{bmatrix}=\left[J\right]^{-1}\begin{bmatrix}\frac{\partial N_1}{\partial\xi}&\frac{\partial N_2}{\partial\xi}&\cdots&\frac{\partial N_8}{\partial\xi}\\\frac{\partial N_1}{\partial\eta}&\frac{\partial N_2}{\partial\eta}&\cdots&\frac{\partial N_8}{\partial\eta}\\\frac{\partial N_1}{\partial\varsigma}&\frac{\partial N_2}{\partial\varsigma}&\cdots&\frac{\partial N_8}{\partial\varsigma}\end{bmatrix}\begin{bmatrix}h_1\\h_2\\\vdots\\h_3\end{bmatrix} \tag{22}$$

where: $\left[J\right]$ is the Jacobi matrix with the expression:

$$[J]=\begin{bmatrix}\frac{\partial x}{\partial\xi}&\frac{\partial y}{\partial\xi}&\frac{\partial z}{\partial\xi}\\\frac{\partial x}{\partial\eta}&\frac{\partial y}{\partial\eta}&\frac{\partial z}{\partial\eta}\\\frac{\partial x}{\partial\zeta}&\frac{\partial y}{\partial\zeta}&\frac{\partial z}{\partial\zeta}\end{bmatrix}=\begin{bmatrix}\sum\limits_{i=1}^{8}\frac{\partial N_i}{\partial\xi}x_i&\sum\limits_{i=1}^{8}\frac{\partial N_i}{\partial\xi}y_i&\sum\limits_{i=1}^{8}\frac{\partial N_i}{\partial\xi}z_i\\\sum\limits_{i=1}^{8}\frac{\partial N_i}{\partial\eta}x_i&\sum\limits_{i=1}^{8}\frac{\partial N_i}{\partial\eta}y_i&\sum\limits_{i=1}^{8}\frac{\partial N_i}{\partial\eta}z_i\\\sum\limits_{i=1}^{8}\frac{\partial N_i}{\partial\zeta}x_i&\sum\limits_{i=1}^{8}\frac{\partial N_i}{\partial\zeta}y_i&\sum\limits_{i=1}^{8}\frac{\partial N_i}{\partial\zeta}z_i\end{bmatrix} \tag{23}$$

There is the following relationship between the parametric coordinate system and the original coordinate system:

$$dxdydz = |J|\, d\xi d\eta d\varsigma \tag{24}$$

where: $|J|$ is the determinant of the Jacobi matrix.

Substituting Eqs. (20), (21), (22), and (23) into Eq. (17) and solving the derivatives of I_1^e, I_2^e, I_3^e to find the minima, respectively, we have:

$$\begin{aligned}
\frac{\partial I_1^e}{\partial\{h\}^e} &= \frac{\partial}{\partial\{h\}^e}\iiint\limits_e \frac{1}{2}\left[k_x\left(\frac{\partial h}{\partial x}\right)^2 + k_y\left(\frac{\partial h}{\partial y}\right)^2 + k_z\left(\frac{\partial h}{\partial x}\right)^2\right]dxdydz \\
&= \frac{\partial}{\partial\{h\}^e}\iiint\limits_e \frac{1}{2}\left[k_x\left(\frac{\partial([N]\{h\}^e)}{\partial x}\right)^2 + k_y\left(\frac{\partial([N]\{h\}^e)}{\partial y}\right)^2 + k_z\left(\frac{\partial([N]\{h\}^e)}{\partial z}\right)^2\right]dxdydz \\
&= \iiint\limits_e \left(\left[\frac{\partial[N]}{\partial x}k_x\frac{\partial[N]^e}{\partial x} + \frac{\partial[N]}{\partial y}k_y\frac{\partial[N]^T}{\partial y} + \frac{\partial[N]}{\partial z}k_z\frac{\partial[N]^T}{\partial z}\right]\right)dxdydz\cdot\{h\}^e \\
&= \int_{-1}^{1}\int_{-1}^{1}\int_{-1}^{1}\left(\left[\frac{\partial[N]}{\partial x}k_x\frac{\partial[N]^T}{\partial x} + \frac{\partial[N]}{\partial y}k_y\frac{\partial[N]^T}{\partial y} + \frac{\partial[N]}{\partial z}k_z\frac{\partial[N]^T}{\partial z}\right]\right)|J|\,d\xi d\eta d\varsigma\cdot\{h\}^e \\
&= [K]^T\{h\}^e
\end{aligned} \tag{25}$$

where: $k_{ij}^e = \int_{-1}^{1}\int_{-1}^{1}\int_{-1}^{1}(k_x\frac{\partial N_i}{\partial x}\frac{\partial N_j}{\partial x} + k_y\frac{\partial N_i}{\partial y}\frac{\partial N_j}{\partial y} + k_z\frac{\partial N_i}{\partial z}\frac{\partial N_j}{\partial z})|J|\,d\xi d\eta d\varsigma$.

$$\begin{aligned}
\frac{\partial I_e^e}{\partial\{h\}^e} &= \frac{\partial}{\partial\{h\}^e}\iiint\limits_e S_s h\frac{\partial h}{\partial t}dxdydz \\
&= \frac{\partial}{\partial\{h\}^e}\iiint\limits_e \left[[N]\{h\}^e\right]\frac{\partial\left[[N]\{h\}^e\right]}{\partial t}dxdydz \\
&= \iiint\limits_e \left[[N]^T S_s [N]\right]dxdydz\cdot\left\{\frac{\partial h}{\partial t}\right\}^e \\
&= \int_{-1}^{1}\int_{-1}^{1}\int_{-1}^{1}\left[[N]^T S_s [N]\right]J\cdot d\xi d\eta d\xi\cdot\left\{\frac{\partial h}{\partial t}\right\}^e = [S_h]^e\left\{\frac{\partial h}{\partial t}\right\}^e
\end{aligned} \tag{26}$$

where: $s_{ij}^e = \int_{-1}^{1}\int_{-1}^{1}\int_{-1}^{1}\int_{-1}^{1} S_s N_i N_j\,|J|\,d\xi d\eta d\varsigma$.

For impermeable boundaries, the flow rate is zero and the third term need not be considered. The discussion here focuses on the variable free surface boundary, which is viewed as a flow replenishment relation for the second type of boundary condition Γ_2, yielding:

$$q = \mu[N]\left\{\frac{\partial h^e}{\partial t}\right\}^e\cos\theta \tag{27}$$

where: h^e is the head on the free surface of the seepage, μ is the effective porosity or degree of water giving to the soil within the range of variation of the free surface of the seepage, and θ is the angle between the outer normal of the free surface of the seepage and the plumb line:

$$\begin{aligned}\frac{\partial I_3^e}{\partial\{h\}^e} &= \frac{\partial}{\partial\{h\}^e}\iint_{\Gamma_4^e} qhd\Gamma \\ &= \iint_{\Gamma_4^e}\frac{\partial}{\partial\{h\}^e}\left(\mu[N]\left\{\frac{\partial h_t^e}{\partial t}\right\}^e\cos\theta[N]\{h\}^e\right)d\Gamma \\ &= \iint_{\Gamma_4^e}\mu[N]^T[N]\cos\theta d\Gamma\cdot\left\{\frac{\partial h^e}{\partial t}\right\}^e = [G]^e\cdot\left\{\frac{\partial h^e}{\partial t}\right\}^e\end{aligned} \tag{28}$$

Eq. $g_{ij}^e = \iint_{\Gamma_4^e}\mu N_i N_j\cos\theta d\Gamma$.

Thus, summing Eq. (25), Eq. (26), and Eq. (27) gives:

$$\left\{\frac{\partial I}{\partial h}\right\}^e = [K]^e\{h\}^e + [S]^e\{\frac{\partial h}{\partial t}\}^e + [G]^e\left\{\frac{\partial h}{\partial t}\right\}^e \tag{29}$$

The above equation has a third term only for unsteady seepage free surface boundary cells.

The system of equations in which the generalized function is differentiated with respect to the nodal head is obtained by superposing the generalized functions for all cells and making them equal to 0 (for a very small value):

$$\left\{\frac{\partial I}{\partial h}\right\} = \sum_{e=1}^{n}([K]^e\{h\}^e + [S]^e\left\{\frac{\partial h}{\partial t}\right\}^e + [G]^e\left\{\frac{\partial h}{\partial t}\right\}^e) = 0 \tag{30}$$

where: n is the total number of nodes: $\sum_{e=1}^{n}$ denotes summing over all cells.

Write the above overall equation in matrix form as:

$$[K]\{h\} + [S]\left\{\frac{\partial h}{\partial t}\right\} + [G]\left\{\frac{\partial h}{\partial t}\right\} = \{F\} \tag{31}$$

where: $[F]$ is the flow array with known nodal heads, internal source-sink terms and flow boundaries contributing to the calculation.

The above finite element solution equation (31) is actually a system of first-order nonlinear differential equations for solving the distribution of pressure head in the computational domain Ω. Since none of the items in Eq. (31) contains the time variable t except for the array $\left\{\frac{\partial}{h}\partial t\right\}$, Eq. (31) is A system of ordinary differential equations with respect to the time variable t, multiplied simultaneously by dt for both its sides and integrated from t^{k-1} to t^k, gives:

$$\int_{t-1}^{t}[K]\{h\}dt + \int_{t-1}^{t}[S]\left\{\frac{\partial h}{\partial t}\right\}dt + \int_{t-1}^{t}[G]\left\{\frac{\partial h}{\partial t}\right\}dt = \int_{t-1}^{t}\{F\}dt \tag{32}$$

Eq. (32) [K], [S], [G], {F} do not contain the time variable t, then [K], [S], [G], {F} can be proposed accordingly before the integral number, let from t^{k-1} to t^k integral corresponds to the first k time step iteration calculation results, in the first k step iteration before the first k step iterative calculations are carried out the first $(k-1)$ time step The results of the iterative calculations are known, and the $k=1$ time step corresponds to the initial value of the seepage pressure head.

When the iteration time period $\Delta^k = t^k - t^{k-1}$ is sufficiently small, it can be assumed:

$$\int_{t-1}^{t}\{h(t)\}dt = \{\bar{h}(t)\}\Delta t \tag{33}$$

Also, for the 2nd term on the left side of Eq. (33):

$$\int_{t-1}^{t}\left\{\frac{\partial h}{\partial t}\right\}dt = \{h^k - h^{k-1}\} \tag{34}$$

Substituting Eqs. (33) and (34) into Eq. (32) yields:

$$[K]\{\bar{h}\}+[S]\frac{\{h^k\}-\{h^{k-1}\}}{\Delta t^k}+[G]\frac{\{h^k\}-\{h^{k-1}\}}{\Delta t^k}=\{F\} \tag{35}$$

In groundwater calculations, when the water level changes slowly during the iteration period Δr^k, $\bar{h}$ can be written in the following form:

$$\{\bar{h}\}=\theta\{h^k\}+(1-\theta)\{h^{k-1}\} \tag{36}$$

Substituting Eq. (36) into Eq. (35) gives:

$$[K][\theta\{h^k\}+(1-\theta)\{h^{k-1}\}]+[S]\frac{\{h^k\}-\{h^{k-1}\}}{\Delta t^k}+[G]\frac{\{h^k\}-\{h^{k-1}\}}{\Delta t^k}=\{F\},0\le\theta\le 1 \tag{37}$$

Following the iterative format, Eq. (37) can be transformed into:

$$\left(\theta[K]+\frac{[S]}{\Delta t^k}+\frac{[G]}{\Delta t^k}\right)\{h^k\}=\{F\}-(1-\theta)[K]\{h^{k-1}\}+\frac{[S]\{h^{k-1}\}}{\Delta t^k}+\frac{[G]\{h^{k-1}\}}{\Delta t^k} \tag{38}$$

III. A. 2) Finite element governing equations for the Beale consolidation theory

Consider the Galyokin weighted residual method to establish the finite element control equation of the Bio-solidification theory, both sides of the same multiplication by the form function $N,(j=1,2,\cdots,n)$, for the entire computational domain integral, its weighted residual integral is 0, to x direction as an example of the analysis can be obtained [22]:

$$\iiint\limits_{\Omega}\left[-G\nabla^2 w_x-\frac{G}{1-2\nu}\frac{\partial}{\partial x}\left(\frac{\partial w_z}{\partial x}+\frac{\partial w_y}{\partial y}+\frac{\partial w_z}{\partial z}\right)+\frac{\partial u}{\partial x}\right]N_j dxdydz=0 \tag{39}$$

From the stepwise integration formula, we have:

$$\begin{aligned}&\iiint\limits_{\Omega}\left[G\left(\frac{\partial w_x}{\partial x}\frac{\partial N_j}{\partial x}+\frac{\partial w_x}{\partial y}\frac{\partial N_j}{\partial y}+\frac{\partial w_x}{\partial z}\frac{\partial N_j}{\partial z}\right)+\frac{G}{1-2\nu}\left(\frac{\partial w_z}{\partial x}+\frac{\partial w_y}{\partial y}+\frac{\partial w_z}{\partial z}\right)\frac{\partial N_j}{\partial x}+\frac{\partial u}{\partial x}N_j\right]dxdydz\\&+\oiint\limits_{\Gamma}\left[G\left(\frac{\partial w_x}{\partial x}+\frac{\partial w_x}{\partial y}+\frac{\partial w_x}{\partial z}\right)+\frac{G}{1-2\nu}\left(\frac{\partial w_x}{\partial x}+\frac{\partial w_y}{\partial y}+\frac{\partial w_z}{\partial z}\right)\right]N_j d\Gamma=0\end{aligned} \tag{40}$$

The integral of the strain over the boundary in the second term at the left end of Eq. (40) is usually zero, and the above equation can be simplified to:

$$\iiint\limits_{\Omega}\left[G\left(\frac{\partial w_s}{\partial x}\frac{\partial N_j}{\partial x}+\frac{\partial w_s}{\partial y}\frac{\partial N_j}{\partial y}+\frac{\partial w_s}{\partial z}\frac{\partial N_j}{\partial z}\right)+\frac{G}{1-2\nu}\left(\frac{\partial w_s}{\partial x}+\frac{\partial w_s}{\partial y}+\frac{\partial w_s}{\partial z}\right)\frac{\partial N_j}{\partial x}+\frac{\partial u}{\partial x}N_j\right]dxdydz=0 \tag{41}$$

As in the previous section, the same form function and coordinate transformation equations are taken as an example for a spatial 8-node isotropic hexahedral linear cell, see Eqs. (18) and (20). For a point within the cell, the displacement and pore pressure modes are:

$$\begin{Bmatrix}w_x\\w_y\\w_z\end{Bmatrix}=\begin{bmatrix}N_1I & N_2I & \cdots & N_8I\end{bmatrix}\begin{Bmatrix}\delta_1^T\\\delta_2^T\\\vdots\\\delta_8^T\end{Bmatrix} \tag{42}$$

$$u=\begin{bmatrix}N_1 & N_2 & \cdots & N_8\end{bmatrix}\begin{Bmatrix}u_1\\u_2\\\vdots\\u_8\end{Bmatrix} \tag{43}$$

where: $I=\begin{bmatrix}1&0&0\\0&1&0\\0&0&1\end{bmatrix},\delta_i=\begin{bmatrix}w_{xi}&w_{yi}&w_{yi}\end{bmatrix}^T\ (i=1,2,\cdots,8),N_i\,(i=1,2,\cdots,8)$ is the spatial eight-node hexahedral unit shape function, the expression of which is given in Eq. (19).

Substituting Eq. (42) and Eq. (43) into Eq. (41) and performing spatial discretization, we obtain:

$$\begin{gathered}\sum_{e=1}^{n}\iiint_e\Bigg[G\left(\frac{\partial N_j}{\partial x}\sum_{i=1}^{8}\frac{\partial N_i}{\partial x}w_{xi}+\frac{\partial N_j}{\partial y}\sum_{i=1}^{8}\frac{\partial N_i}{\partial y}w_{xi}+\frac{\partial N_j}{\partial z}\sum_{i=1}^{8}\frac{\partial N_i}{\partial z}w_{xi}\right)\\+\frac{G}{1-2v}\frac{\partial N_j}{\partial x}\sum_{i=1}^{8}\left(\frac{\partial N_i}{\partial x}w_{xi}+\frac{\partial N_i}{\partial y}w_{yi}+\frac{\partial N_i}{\partial z}w_{zi}\right)+N_j\sum_{i=1}^{8}\frac{\partial N_i}{\partial x}u_i\Bigg]dxdydz=0\\\left(j=1,2,\cdots,8\right)\end{gathered}\tag{44}$$

Similarly for y and z directions:

$$\begin{gathered}\sum_{e=1}^{n}\iiint_e\Bigg[G\left(\frac{\partial N_j}{\partial x}\sum_{i=1}^{8}\frac{\partial N_i}{\partial x}w_{yi}+\frac{\partial N_j}{\partial y}\sum_{i=1}^{8}\frac{\partial N_i}{\partial y}w_{yi}+\frac{\partial N_j}{\partial z}\sum_{i=1}^{8}\frac{\partial N_i}{\partial z}w_{yi}\right)\\+\frac{G}{1-2v}\frac{\partial N_j}{\partial y}\sum_{i=1}^{8}\left(\frac{\partial N_i}{\partial x}w_{xi}+\frac{\partial N_i}{\partial y}w_{yi}+\frac{\partial N_i}{\partial z}w_{zi}\right)+N_j\sum_{i=1}^{8}\frac{\partial N_i}{\partial y}u_i\Bigg]dxdydz=0\\\left(j=1,2,\cdots,8\right)\end{gathered}\tag{45}$$

$$\begin{gathered}\sum_{e=1}^{n}\iiint_e\Bigg[G\left(\frac{\partial N_j}{\partial x}\sum_{i=1}^{8}\frac{\partial N_i}{\partial x}w_{zt}+\frac{\partial N_j}{\partial y}\sum_{i=1}^{8}\frac{\partial N_i}{\partial y}w_{zt}+\frac{\partial N_j}{\partial z}\sum_{i=1}^{8}\frac{\partial N_i}{\partial z}w_{zt}\right)\\\frac{G}{1-2v}\frac{\partial N_j}{\partial y}\sum_{i=1}^{8}\left(\frac{\partial N_i}{\partial x}w_{xi}+\frac{\partial N_i}{\partial y}w_{yi}+\frac{\partial N_i}{\partial z}w_{zi}\right)+N_j\sum_{i=1}^{8}\frac{\partial N_i}{\partial z}u_i\Bigg]dxdydz=0\\\left(j=1,2,\cdots,8\right)\end{gathered}\tag{46}$$

Writing equations (44), (45) and (46) in matrix form, there are:

$$[K]\{\delta\}+[C]\{u\}=\{F\}\tag{47}$$

In the formula:

$K_{ij}=\sum_{e=1}^{n}\iiint_e[B_i]^T[D][B_j]dxdydz$,

$C_{ij}=\sum_{e=1}^{n}\iiint_e[B_i]^T[M]N_j dxdydz$,

$\{M\}=\begin{bmatrix}1&1&1&0&0&0\end{bmatrix}^r$,

$B_i=\begin{bmatrix}\frac{\partial N_i}{\partial x}&0&0&\frac{\partial N_i}{\partial y}&0&\frac{\partial N_i}{\partial z}\\0&\frac{\partial N_i}{\partial y}&0&\frac{\partial N_i}{\partial x}&\frac{\partial N_i}{\partial z}&0\\0&0&\frac{\partial N_i}{\partial z}&0&\frac{\partial N_i}{\partial y}&\frac{\partial N_i}{\partial x}\end{bmatrix}(i=1,2,\cdots,8)$,

F_i is the equivalent load array for i nodes.

Still taking $N_j\,(j=1,2,\cdots,n)$ as the form function, multiplying both sides by the form function $N_j\,(j=1,2,\cdots,n)$, and integrating over the whole computational domain by using the weighted residual method, which integrates over the whole computational domain with a weighted residual of 0, we can obtain:

$$\iiint_{\Omega}\left\{-\frac{\partial}{\partial t}\left(\frac{\partial w_z}{\partial x}+\frac{\partial w_y}{\partial y}+\frac{\partial w_z}{\partial z}\right)+\frac{1}{\gamma_w}\left[\frac{\partial}{\partial x}\left(k_x\frac{\partial u}{\partial x}\right)+\frac{\partial}{\partial y}\left(k_y\frac{\partial u}{\partial y}\right)+\frac{\partial}{\partial z}\left(k_z\left(\frac{\partial u}{\partial z}+\gamma_w\right)\right)\right]\right\}N_j dxdydz=0 \tag{48}$$

Integration by parts and use of the Gaussian formula gives:

$$\begin{aligned}&\iiint_{\Omega}\left[-\frac{\partial}{\partial t}\left(\frac{\partial w_z}{\partial x}+\frac{\partial w_y}{\partial y}+\frac{\partial w_z}{\partial z}\right)N_j-\frac{1}{\gamma_w}\left(\frac{\partial u}{\partial x}k_x\frac{\partial N_j}{\partial x}+\frac{\partial u}{\partial y}k_y\frac{\partial N_j}{\partial y}+\frac{\partial u}{\partial z}k_z\frac{\partial N_j}{\partial z}\right)\right]dxdydz\\&+\oiint_{\Gamma}\frac{1}{\gamma_w}\left(k_x\frac{\partial u}{\partial x}+k_y\frac{\partial u}{\partial y}+k_z\frac{\partial u}{\partial z}\right)N_j d\Gamma=0\end{aligned} \tag{49}$$

Eq. (49) is obtained after spatial discretization:

$$\begin{aligned}&\sum_{e=1}^{n}\iiint_{e}\left[\frac{\partial}{\partial t}\left(\frac{\partial w_x}{\partial x}+\frac{\partial w_y}{\partial y}+\frac{\partial w_z}{\partial z}\right)N_j+\frac{1}{\gamma_w}\left(\sum_{i=1}^{8}\frac{\partial N_i}{\partial x}k_x\frac{\partial N_j}{\partial x}\cdot u_i+\sum_{i=1}^{8}\frac{\partial N_i}{\partial y}k_y\frac{\partial N_j}{\partial y}\cdot u_i\right.\right.\\&\left.\left.+\sum_{i=1}^{8}\frac{\partial N_i}{\partial z}k_z\frac{\partial N_j}{\partial z}\cdot u_i\right)\right]dxdydz-\oiint_{\Gamma}\frac{1}{\gamma_w}\left(\sum_{i=1}^{8}k_x\frac{\partial N_i}{\partial x}\cdot u_i+\sum_{i=1}^{8}k_y\frac{\partial N_i}{\partial y}\cdot u_i+\sum_{i=1}^{8}k_z\frac{\partial N_i}{\partial z}\cdot u_i\right)N_j d\Gamma=0\end{aligned} \tag{50}$$

Writing equation (50) in matrix form, we have:

$$[C]^r\left\{\frac{\partial\delta}{\partial t}\right\}+[H]\{u\}=\{Q\} \tag{51}$$

In the formula:

$$H_y=\sum_{e=1}^{n}\iiint_{e}[B_n]^T[k]\left[B_y\right]dxdydz\ ,$$

$$B_{si}=\left[\frac{\partial N_i}{\partial x}\ \frac{\partial N_i}{\partial y}\ \frac{\partial N_i}{\partial z}\right]^T,$$

Q_i is the equivalent flow array at i nodes.

For the free surface problem, the same method as for the percolation flow is applied to the free surface in conjunction with its fixed solution conditions to obtain:

$$\begin{aligned}&\iiint_{\Omega}\left\{-\frac{\partial}{\partial t}\left(\frac{\partial w_x}{\partial x}+\frac{\partial w_y}{\partial y}+\frac{\partial w_z}{\partial z}\right)+\frac{1}{\gamma_w}\left[\frac{\partial}{\partial x}\left(k_x\frac{\partial u}{\partial x}\right)+\right.\right.\\&\left.\left.\frac{\partial}{\partial y}\left(k_y\frac{\partial u}{\partial y}\right)+\frac{\partial}{\partial z}\left(k_z\left(\frac{\partial u}{\partial z}+\gamma_w\right)\right)\right]+\iint_{\Gamma_4}qd\Gamma\right\}N_j dxdydz=0\end{aligned} \tag{52}$$

Taking a similar approach to Eq. (52) yields:

$$[C]^T\left\{\frac{\partial\delta}{\partial t}\right\}+[H]\{u\}+[G]\left\{\frac{\partial u}{\partial t}\right\}=\{Q\} \tag{53}$$

Eq. $G_{ij}=\iint_{\Gamma_i}N_t\frac{\mu\cos\theta}{\gamma}N_j d\Gamma$.

Differencing the times in Eq. (53) yields:

$$[C]^T\{\delta\}+\theta\Delta t[H]\{u\}+[G]\{u\}=\{\theta\Delta tQ\} \tag{54}$$

The Biot 3D consolidation finite element equation can be obtained by associating Eqs. (47) and (54) as:

$$\begin{bmatrix}K & C\\ C^T & \theta\Delta tH+G\end{bmatrix}\begin{Bmatrix}\delta\\ u\end{Bmatrix}=\begin{Bmatrix}F\\ \theta\Delta tQ\end{Bmatrix} \tag{55}$$

Although the Beale consolidation equation assumes that the skeleton is linearly elastic in its derivation, with the finite unit method, it can be generalized and applied to nonlinear problems by introducing an elasto-plastic stress-strain relationship, at which point it will be more convenient to take the displacement increment during the Δt time period in the basic unknowns in place of the displacement, and then Eq. (55) can be rewritten as follows:

$$\begin{bmatrix} K & C \\ C^T & \theta\Delta tH+G \end{bmatrix} \begin{Bmatrix} \Delta\delta \\ \Delta u \end{Bmatrix} = \begin{Bmatrix} \Delta F \\ \theta\Delta t\Delta Q \end{Bmatrix} \tag{56}$$

If the pore pressure is expressed in the form of a full quantity, noting that the full quantity of the pore pressure of the unit node i at the moments t_n and t_{n+1} are $u_i(n)$ and $u_{i(n+1)}$, respectively, and $\Delta u_i = u_{i(n+1)} - u_{i(n)}$, then Eq. (57) can be transformed as:

$$\begin{bmatrix} K & C \\ C^T & \theta\Delta tH+G \end{bmatrix} \begin{Bmatrix} \Delta\delta \\ u_{i(n+1)} \end{Bmatrix} = \begin{Bmatrix} \Delta F + Cu_{i(n)} \\ \theta\Delta t\Delta Q - (\theta\Delta tH+G)u_{i(n)} \end{Bmatrix} \tag{57}$$

If the seepage effect caused by the difference in head between the inside and outside of the pit is considered, it is appropriate to analyze it in terms of the total head potential U (expressed in the form of pore pressure). The formula for the total head potential (with the spatial coordinate z upward positive) is:

$$U = u + \gamma_w z = u_0 + u' + \gamma_w z \tag{58}$$

where u_0, u' and $\gamma_w z$ are the hydrostatic pressure, the superhydrostatic pore pressure, and the positional head potential, respectively.

When expressed in terms of total head, the total head potential of cell node i at moment t_{n+1} is noted as $U_i(n+1)$, and the hydrostatic and superhydrostatic pore pressures of cell node i at moment t_n are $U_{0i(n)}$ and $U'_{i(n)}$, respectively, without considering the vertical displacement effect (i.e., the positional head potential $\gamma_w z$ is constant), then Eq. (57) can be transformed as:

$$\begin{bmatrix} K & C \\ C^T & \theta\Delta tH+G \end{bmatrix} \begin{Bmatrix} \Delta\delta \\ U_{i(n+1)} \end{Bmatrix} = \begin{Bmatrix} \Delta F + C(U_{0i(n)} + U'_{i(n)} + \gamma_w z) \\ \theta\Delta t\Delta Q - (\theta\Delta tH+G)(U_{0i(n)} + U'_{i(n)} + \gamma_w z) \end{Bmatrix} \tag{59}$$

III. B. Model Identification and Validation

III. B. 1) Groundwater Flow Model Identification

In order to check whether the identified model hydrogeological parameters are reasonable and reliable, the identified model and hydrogeological parameters were used to calculate the groundwater level and soil deformation in other time periods and compared with the measured data to check the model.

The observed data of groundwater level in the validation period (February 2013 to February 2014) are used to check whether the identified model hydrogeological parameters are reasonable. Figure 1 shows a schematic diagram of the water level fit for the Ⅰ aquifer during the validation period, with observation well 24 in Figure (a), observation well G203 in Figure (b), observation well G207F in Figure (c), and observation well G208 in Figure (d), to validate the water level fit for observation wells in the Ⅰ and the pressurized aquifer.The differences between the observed values and the computed values for observation wells 24 and G207F are small, with the largest differences of 1.2 and 0.96. The water level in observation well G208 is the smallest, ranging from -1.6 to -0.75 under the calculated values.

III. B. 2) Identification of soil deformation models

The stratified marker monitoring data of the subsidence center within the validation period (February 2013 to February 2014) were used to test whether the identified model hydrogeological parameters were reasonable. Figure 2 shows the calculated and observed values of the cumulative deformation of each soil layer in the ground settlement center during the validation period, the model has a high accuracy for the identification of soil deformation, in which the two differences for ground settlement are the largest, 1.2.

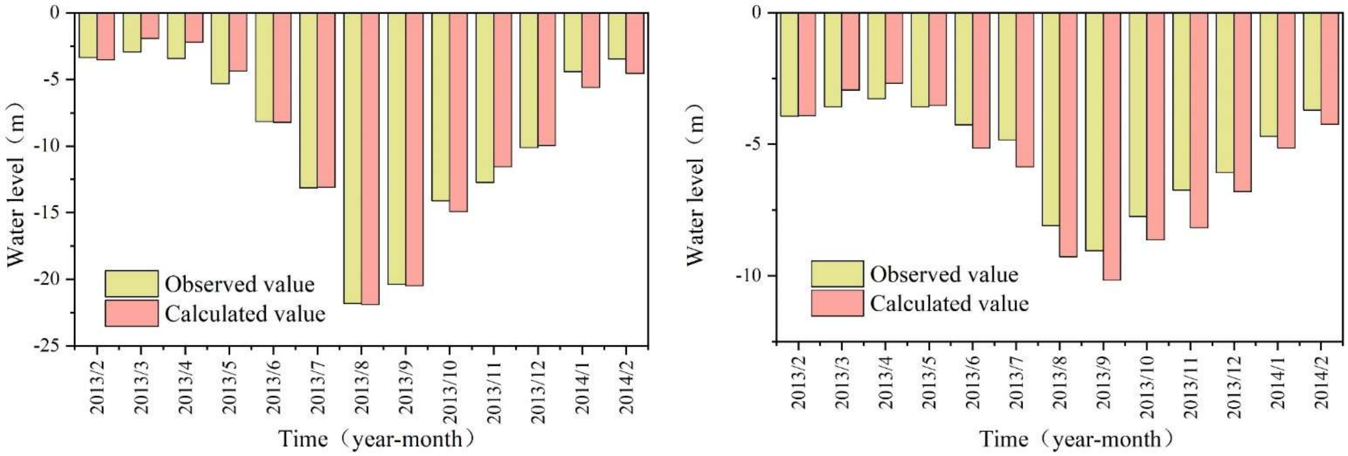

(a)Observation Well 24

(b)Observation Well G203

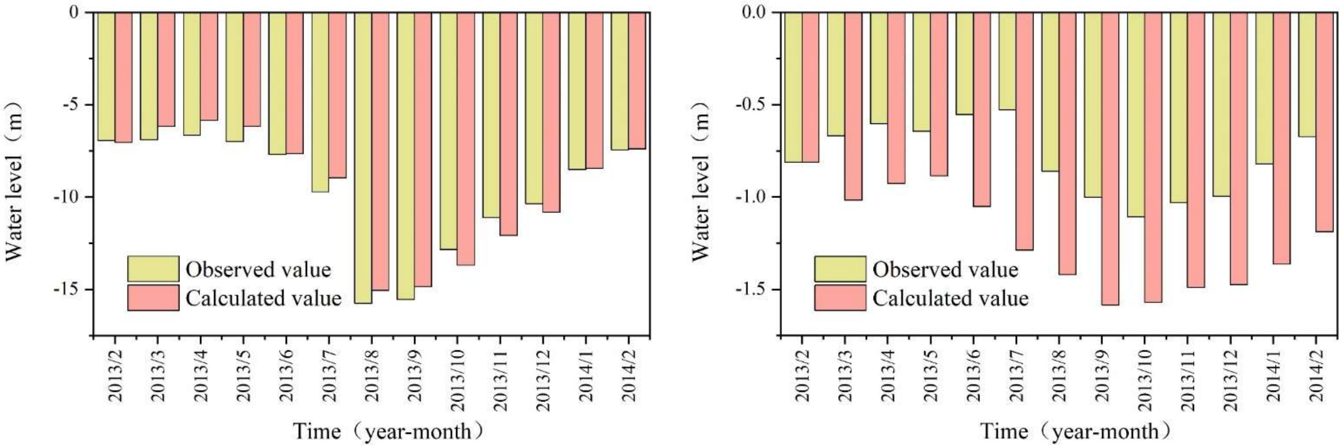

(c)Observation Well G207F

(d)Observation Well G208

Figure 1: Schematic diagram of water level fitting of the Ⅰ aquifer in the verification period

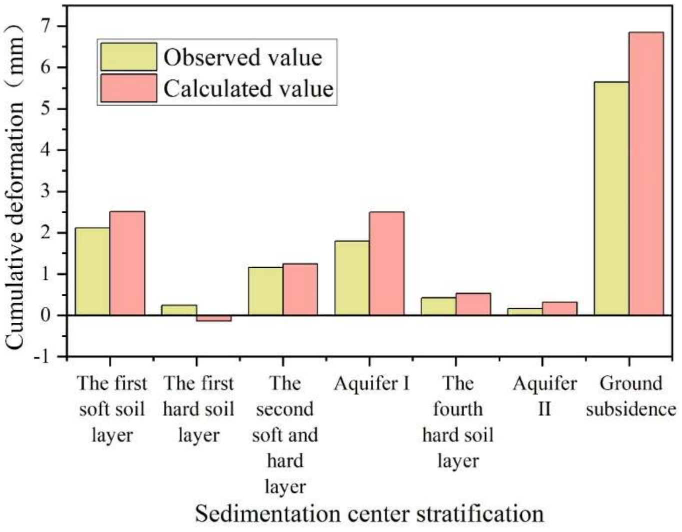

Figure 2: The accumulation of soil in the ground subsidence center

III. B. 3) Model parameter identification

According to the method of model identification, the model hydrogeological parameters are identified and calibrated by using the groundwater level observation data and subsidence center stratification marker monitoring data during the identification period (February 2012 to February 2013), and the model hydrogeological parameters that fit well with the actual observation values are obtained. The recognized hydrogeological parameters of the groundwater flow model are shown in Table 1, and the storage rate (S_s (1/m)) of the Ⅰ pressurized aquifer is slightly higher than that of the Ⅱ pressurized aquifer, and the average value of the zonal storage rate is 0.00007385, which is 0.00002048 higher than that of the Ⅱ pressurized aquifer.

Table 1: Hydrogeological parameters of groundwater flow model

Ⅰ confined aquifer				Ⅱ Confined Aquifer			
Partition number	K_h(m/d)	K_h/k_v	S_s(1/m)	Partition number	K_h(m/d)	K_h/k_v	S_s(1/m)
1	23	4	0.00008	1	15	5	0.000048
2	15	4	0.000098	2	12	5	0.000051
3	13	4	0.000067	3	10	5	0.000053
4	5	4	0.00009	4	6	5	0.000048
5	10	4	0.000067	5	3.3	5	0.000068
6	3	4	0.000078	6	4	5	0.000052
7	2.5	4	0.000095	7	4	5	0.000083
8	2.5	4	0.000068	8	4.5	5	0.000065
9	5.5	4	0.000085	9	2	5	0.000054
10	3	4	0.000065	10	1	5	0.000062
11	2	4	0.000085	11	0.00031	5	0.000003
12	4.5	4	0.000079				
13	0.00024	4	0.000003				

Table 2 shows the error statistics of the simulation results of ground settlement from 2012-2013, and the fitting analysis shows that the simulation results of soil deformation in the HM area of NT city are better, and for the area around the HM, it is difficult to calculate the exact depth of water level drop and the settlement value better because the soil deformation area is located at the boundary. In this study, 24 stratigraphic scale ground settlement monitoring points were selected, and the error analysis of the simulated and measured values of ground settlement in 2012-2013 was conducted: 19 of them reached within ±20mm error, accounting for 79.167% of the total monitoring points.

Table 2: 2012-2013 ground subsidence volume simulation results error

Layering label	Measured value (mm)	Analog value (mm)	Error value (mm)	Layering label	Measured value (mm)	Analog value (mm)	Error value (mm)
Ⅱ07	78	60	18	GPS01	-12	6	-18
Ⅱ08	20	32	-12	GPS09	65	60	5
Ⅱ12	65	81	-16	GPS10	70	54	16
Ⅱ13	15	24	-9	GPS14	20	15	5
Ⅱ24	5	18	-13	GPS15	3	11	-8
Ⅱ28	23	13	10	GPS32	25	4	21
Ⅱ31	29	35	-6	GPS39	5	25	-20
Ⅱ32	40	17	23	GPS45	20	15	5
Ⅱ33	38	20	18	GPS46	13	40	-27
Ⅱ35	35	23	12	GPS53	-20	5	-25
Ⅱ36	43	30	13	GPS54	-11	6	-17
Ⅱ37	48	55	-7	RS01	28	55	-27

IV. Coupled analysis of groundwater flow-soil deformation in geotechnical engineering

IV. A. Soil-moisture deformation coupling

The relationship between the average water content of each soil layer and the deformation of the soil layer at different moments during precipitation is shown in Fig. 3, with the upper sandy soil layer in Fig. (a), the middle clay layer in Fig. (b) and the lower sandy soil layer in Fig. (c). During the precipitation stage, with the decrease of the average water content of each soil layer, the soil layer was compressed and deformed accordingly. The average water content and vertical deformation of the upper sandy-soil layer were highly consistent with each other, with the average water content decreasing from 27% to 13% and the average compressive deformation decreasing from -0.01mm to -0.14mm from 0 to 5h, and the moisture and deformation of the upper sandy-soil layer were in a stable state after 5h. The average moisture content and vertical deformation of the lower sand layer were basically the same, the average moisture content decreased from 23% to 17% in 0-5h, and was in a stable state after 5h, and the average compression deformation was always in an increasing state, and the rate of increase was from fast to slow. In the middle clay layer, the compression deformation rate is lower than the average water content reduction rate in 0-2h, the average water content reduction rate decreases slowly in 2-8h, and the compression deformation rate is accelerated suddenly, and the water in the viscous upper layer is transformed from weakly bonded water to free water and released continuously, and the compression deformation is also mainly concentrated in this stage, moreover, the compression deformation rate of the viscous upper layer is lagging behind that of the average water content reduction rate, and this phenomenon is attributed to the fact that the viscous upper layer has been in a state of transient hyperstatic pore space. This phenomenon is due to the slow dissipation of the transient superstatic pore water pressure on the viscosity.

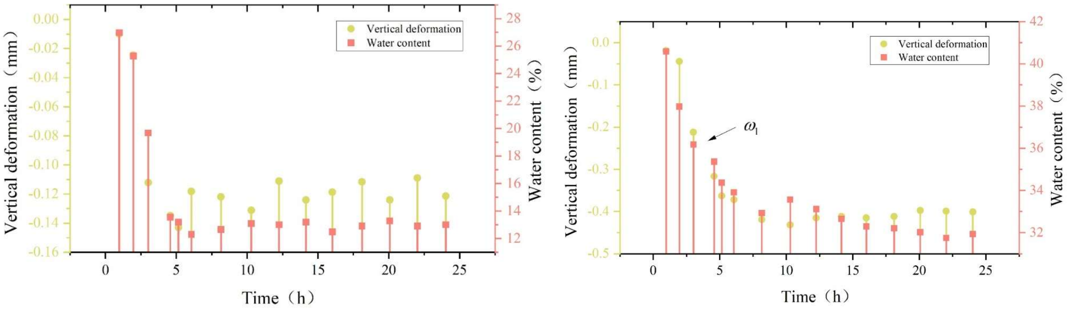

(a)The upper sandy soil layer (b)The clay layer in the middle of the spoon

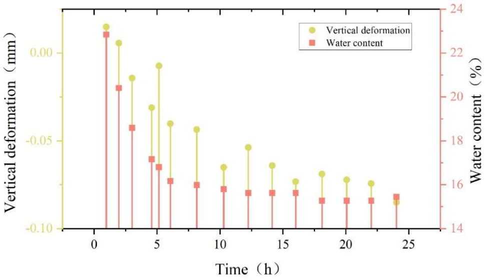

(c)The lower sandy soil layer

Figure 3: The relationship between soil moisture and deformation in the precipitation stage

IV. B. Coupled soil moisture-deformation analysis

In this test, the compression deformation and rebound deformation of the soil body were mainly concentrated in the central clay layer, so the moisture-deformation change relationship of the clay layer was mainly analyzed. Fig. 3 shows that during the precipitation process, the average water content of the clay layer is lower than the liquid limit (ω_l), i.e., the average rate of compressive deformation of the clay layer increases rapidly after the beginning of the precipitation phase for 2 h. The average rate of compressive deformation of the clay layer increases rapidly after the beginning of the precipitation phase.

The phenomenon of ground settlement is closely linked to seepage in the soil, and the coupling of soil moisture and deformation has an important influence on ground settlement. When groundwater is over-extracted, the pore water pressure in the pressurized aquifer decreases and the effective stress increases. The distance between sand particles decreases, which compresses the sand layer. The pore water pressure of the neighboring clay layer rises, forming a hydraulic gradient to the aquifer. The pore water in the clay layer is released, which ultimately leads to the compression and deformation of the clay layer, thus creating a ground settlement hazard. The ground settlement process is also divided into two stages, the first stage is the main compressive deformation stage, caused by the pore water pressure changes due to groundwater extraction. The second stage is the slow compression deformation stage, which is caused by the creep of the soil after pumping. In terms of groundwater recharge, studies have shown that under the same pressure conditions, the recharge volume is only 12-19% of the discharge volume. Therefore, if the process of pumping and recharging is repeated, the soil structure will reach a relatively stable state after two stages of compression deformation, the compression deformation caused by drainage will become smaller and smaller, and the resilient deformation caused by recharging will increase relatively.

V. Conclusion

In this paper, the HM district of NT city is selected as the study area, and the hydrogeological conceptual model is constructed by combining the hydrogeological conditions of the area, and the deformation direction of the soil is simulated according to the Terzaghi effective stress principle. A three-dimensional groundwater flow-one-dimensional soil deformation coupling model is established, and a finite element discrete model is used to solve it.

To verify the identification accuracy of the groundwater flow model and the soil deformation model, during the validation period, the observed values of observation wells 24 and G207F differed from the calculated values in a small way, with the largest differences of 1.2 and 0.96, and the water level in observation well G208 was the smallest, with the water level under the calculated values ranging from -1.6 to -0.75. Meanwhile, the model has a high accuracy in recognizing the deformation of the soil body, with the largest difference between the two for ground settlement at 1.2.

For the coupled analysis of groundwater flow-soil deformation in geotechnical engineering, during the precipitation stage, as the average water content of each soil layer decreases, compressive deformation of the soil layer occurs accordingly. In the upper sandy soil layer, the average water content decreased from 27% to 13% from 0 to 5h, and the average compression deformation decreased from -0.01mm to -0.14mm, and the moisture and deformation of the sandy soil layer were in a stable state after 5h.

References

[1] Sousa, R., Karam, K. S., Costa, A. L., & Einstein, H. H. (2017). Exploration and decision-making in geotechnical engineering–a case study. Georisk: Assessment and Management of Risk for Engineered Systems and Geohazards, 11(1), 129-145.

[2] Al-Arafat, M., Kabi, M. E., Morshed, A. S. M., & Sunny, M. A. U. (2024). Geotechnical Challenges In Urban Expansion: Addressing Soft Soil, Groundwater, And Subsurface Infrastructure Risks In Mega Cities. Innovatech Engineering Journal, 1(01), 205-222.

[3] Li, P. (2025). Analysis of the impact of groundwater seepage on the stability of foundation works in geotechnical engineering. J. COMBIN. MATH. COMBIN. COMPUT, 127, 631-654.

[4] Chaminé, H. I. (2015). Water resources meet sustainability: new trends in environmental hydrogeology and groundwater engineering. Environmental Earth Sciences, 73, 2513-2520.

[5] Hassan, W., Qasim, M., Alshameri, B., Shahzad, A., Khalid, M. H., & Qamar, S. U. (2024). Geospatial intelligence in geotechnical engineering: a comprehensive investigation into SPT-N, soil types, and undrained shear strength for enhanced site characterization. Bulletin of Engineering Geology and the Environment, 83(10), 380.

[6] Sun, L., Wang, X., Wang, S., Sun, W., Wang, J., & Di, H. (2024). Experimental study on soil deformation caused by overexploitation of groundwater. Water Environment Research, 96(9), e11111.

[7] He, G., Yan, X., Zhang, Y., Yang, T., Wu, J., Bai, Y., & Gu, D. (2020). Experimental study on the vertical deformation of soils due to groundwater withdrawal. International Journal of Geomechanics, 20(7), 04020076.

[8] Li, M. G., Chen, J. J., Xia, X. H., Zhang, Y. Q., & Wang, D. F. (2020). Statistical and hydro-mechanical coupling analyses on groundwater drawdown and soil deformation caused by dewatering in a multi-aquifer-aquitard system. Journal of Hydrology, 589, 125365.

[9] Yang, J., Cao, G., Han, D., Yuan, H., Hu, Y., Shi, P., & Chen, Y. (2019). Deformation of the aquifer system under groundwater level fluctuations and its implication for land subsidence control in the Tianjin coastal region. Environmental monitoring and assessment, 191, 1-14.

[10] Khorrami, M., Alizadeh, B., Ghasemi Tousi, E., Shakerian, M., Maghsoudi, Y., & Rahgozar, P. (2019). How groundwater level fluctuations and geotechnical properties lead to asymmetric subsidence: A PSInSAR analysis of land deformation over a transit corridor in the Los Angeles metropolitan area. Remote Sensing, 11(4), 377.

[11] He, X., Shi, W., Zhu, Y., Yan, L., Zhao, Y., & Wang, S. (2025). Coupled Effects of Fault-Related Groundwater Flow and Pore Water Pressure: Unraveling the Mechanisms of Deformation and Failure in Gentle Slopes. Arabian Journal for Science and Engineering, 1-18.

[12] Panda, S. D., Kumar, S., Pradhan, S. P., Singh, J., Kralia, A., & Thakur, M. (2023). Effect of groundwater table fluctuation on slope instability: a comprehensive 3D simulation approach for Kotropi landslide, India. Landslides, 20(3), 663-682.

[13] Ni, P., Mei, G., & Zhao, Y. (2018). Influence of raised groundwater level on the stability of unsaturated soil slopes. International Journal of Geomechanics, 18(12), 04018168.

[14] Wang, X., Deng, Y., Dong, M., Guan, M., Wu, Y., & Xu, R. (2025). A simplified method for evaluating shallow slope stability of slopes based on an indirectly coupled runoff and groundwater seepage model. Hydrogeology Journal, 33(1), 309-327.

[15] Zhang, S., Xu, Q., Peng, D., Zhu, Z., Li, W., Wong, H., & Shen, P. (2020). Stability analysis of rock wedge slide subjected to groundwater dynamic evolution. Engineering geology, 270, 105528.

[16] Ball, J. L., Taron, J., Reid, M. E., Hurwitz, S., Finn, C., & Bedrosian, P. (2018). Combining multiphase groundwater flow and slope stability models to assess stratovolcano flank collapse in the Cascade Range. Journal of Geophysical Research: Solid Earth, 123(4), 2787-2805.

[17] Antoncecchi, I., Ciccone, F., Rossi, G., Agate, G., Colucci, F., Moia, F., ... & Petracchini, L. (2021). Soil deformation analysis through fluid-dynamic modelling and DInSAR measurements. A focus on groundwater withdrawal in the Ravenna area (Italy). BULLETIN OF GEOPHYSICS AND OCEANOGRAPHY, 62(2), 301-318.

[18] Yao, X. (2025). Numerical Simulation Study on the Coupling Model of Groundwater Flow and Soil Deformation in Geotechnical Engineering. J. COMBIN. MATH. COMBIN. COMPUT, 127, 9573-9594.

[19] Bonì, R., Meisina, C., Teatini, P., Zucca, F., Zoccarato, C., Franceschini, A., ... & Herrera, G. (2020). 3D groundwater flow and deformation modelling of Madrid aquifer. Journal of Hydrology, 585, 124773.

[20] Guido Leone,Libera Esposito & Francesco Fiorillo. (2023). Terzaghi's Effective Stress Principle and Hydrological Deformation of Karst Aquifers Detected by GNSS Measurements. Rock Mechanics and Rock Engineering,57(4),2365-2383.

[21] Putritansy Neysa,Heru Hendrayana & Pulung Arya Pranantya. (2025). Preliminary Hydrogeology Conceptual Model of the East Banyuwangi Coastal Plain Area, East Java Province. IOP Conference Series: Earth and Environmental Science,1451(1),012016-012016.

[22] Chunmei Wang,Junping Wang & Shangyou Zhang. (2024). Weak Galerkin finite element methods for optimal control problems governed by second order elliptic equations. Journal of Computational and Applied Mathematics,452,115982-115982.